We are IntechOpen, the world's leading publisher of Open Access books Built by scientists, for scientists

4,800
Open access books available

122,000
International authors and editors

135M
Downloads

Our authors are among the

154
Countries delivered to

TOP 1%
most cited scientists

12.2%
Contributors from top 500 universities

CLARIVATE ANALYTICS BOOK CITATION INDEX INDEXED

WEB OF SCIENCE™

Selection of our books indexed in the Book Citation Index in Web of Science™ Core Collection (BKCI)

Interested in publishing with us?
Contact book.department@intechopen.com

Numbers displayed above are based on latest data collected.
For more information visit www.intechopen.com

9

ZnO Nanostructures for Optoelectronic Applications

Ashok K. Sood[1], Zhong Lin Wang[2], Dennis L. Polla[3], Nibir K. Dhar[3], Tariq Manzur[4] and A.F.M. Anwar[5]

[1]*Magnolia Optical Technologies Inc, 52-B Cummings Park, Suite 314, Woburn, MA 01801*

[2]*School of Materials Science and Engineering, Georgia Institute of Technology, 771 Ferst Drive, Atlanta, GA 30332*

[3]*DARPA /MTO, 3701 North Fairfax Drive, Arlington, VA 22203*

[4]*Naval Underwater Warfare Center, 1176 Howell Street, Newport, RI 02841*

[5]*Department of Electrical Engineering, University of Connecticut, Storrs, CT 06269 U.S.A.*

1. Introduction

ZnO is a unique material that exhibits both semiconducting and piezoelectric properties. ZnO is a unique material that exhibits both Semi conducting and piezoelectric properties. ZnO devices have been demonstrated for applications in piezoelectric pressure sensors and Pyroelectric infrared detectors [1] and Spintronic devices [2]. More recently, there has been significant effort underway for design and development of ZnO nanostructures such as ZnO nanowires for a variety of applications [3-7].

The ZnO nanostructures can be implemented in Optoelectronic, Sensors, Transducers and Biomedical applications [1, 2, 3, 4]. Use of these nanostructures, will allow building of Nanoscale nanosensors, nanocantilevers, field-effect transistors and nanoresonators for a variety of Military, Homeland Security and Commercial Applications. Due to the advancement of materials technology over the past decade, wide-band gap semiconductors such as SiC, GaN and ZnO have emerged as UV sensitive materials that have applications for UV lasers, UV Photodetector, switches, Bio-Sensors and solar cells.

ZnO wide-band gap semiconductor is promising for sensor applications in the UV range. The band-gap is 3.2 eV for ZnO. Therefore, GaN and ZnO, as well as SiC are potentially good materials to cover the UV spectral band (240-280 nm), when solar radiation is completely absorbed by the ozone layer of the earth atmosphere, so the background of solar radiation at the earth surface is essentially zero.

ZnO is transparent to visible light and can be made highly conductive by doping. ZnO is a versatile functional material that has a diverse group of growth morphologies. These growth morphologies have been demonstrated for nanowires (1), nanobelts (2), nanocages (3), nanocombs (4), nanosprings (5), nanorings (6), nanohelixes (7). The objective of this chapter is to review the unique ZnO nanostructure devices and characterized for optoelectronic applications.

2. Crystal structure of ZnO and its polar surfaces

Table 1 lists the basic physical properties of bulk ZnO. It is worth noting that as the dimension of the semiconductor materials continuously shrinks down to nanometer or even smaller scale, some of their physical properties undergo changes known as the "quantum size effects" [8]. For example, quantum confinement increases the band gap energy of quasi-one-dimensional (Q1D) ZnO, which has been confirmed by photoluminescence [8].
Bandgap of ZnO nanoparticles also demonstrates such size dependence. Understanding the fundamental physical properties is crucial to the rational design of functional devices. Investigation of the properties of individual ZnO nanostructures is essential for developing their potential as the building blocks for future nanoscale devices.

Properties	Value
Lattice constants (T = 300 K)	
a_0	0.32469 nm
c_0	0.52069 nm
Density	5.606 g/cm^3
Melting point	2248 K
Relative dielectric constant	8.66
Gap Energy	3.4 eV, direct
Intrinsic carrier concentration	$< 10^6$ cm^{-3}
Exciton binding Energy	60 meV
Electron effective mass	0.24
Electron mobility (T = 300 K)	200 cm^2/V s
Hole effective mass	0.59
Hole mobility (T = 300 K)	5-50 cm^2/V s

Table 1. Physical properties of wurtzite ZnO [Fan et al; Ref 8]

Zinc oxide has a hexagonal structure (space group $P6_3mc$) with lattice parameters a = 0.3296, and c = 0.52065 nm. The structure of ZnO can be simply described as a number of alternating planes composed of tetrahedral coordinated O^{2-} and Zn^{2+} ions, stacked alternatively along the c-axis (Figure 1a). The tetrahedral coordination in ZnO results in non-central symmetric structure and piezoelectricity. Another important characteristic of ZnO is the polar surfaces. The most common polar surface is the basal plane. The oppositely charged ions produce positively charged Zn-(0001) and negatively charged O-$(000\bar{1})$ polar surfaces (Figure 1b), resulting in a normal dipole moment and spontaneous polarization along the c-axis.
Another polar surface is the $\{01\bar{1}1\}$. By projecting the structure along $[1\bar{2}10]$, as shown in Figure 1b, beside the most typical ±(0001) polar surfaces that are terminated with Zn and oxygen, respectively, $\pm(10\bar{1}1)$ and $\pm(10\bar{1}\,\bar{1})$ are also polar surfaces. The $\{10\bar{1}1\}$ type surfaces are not common for ZnO, but they have been observed in a nanohelical structure found recently [9]. The charges on the polar surfaces are ionic charges, which are non-transferable and non-flowable. Because the interaction energy among the charges depends

on the distribution of the charges, the structure is arranged in such a configuration to minimize the electrostatic energy. This is the main driving force for growing the polar surface dominated nanostructures.

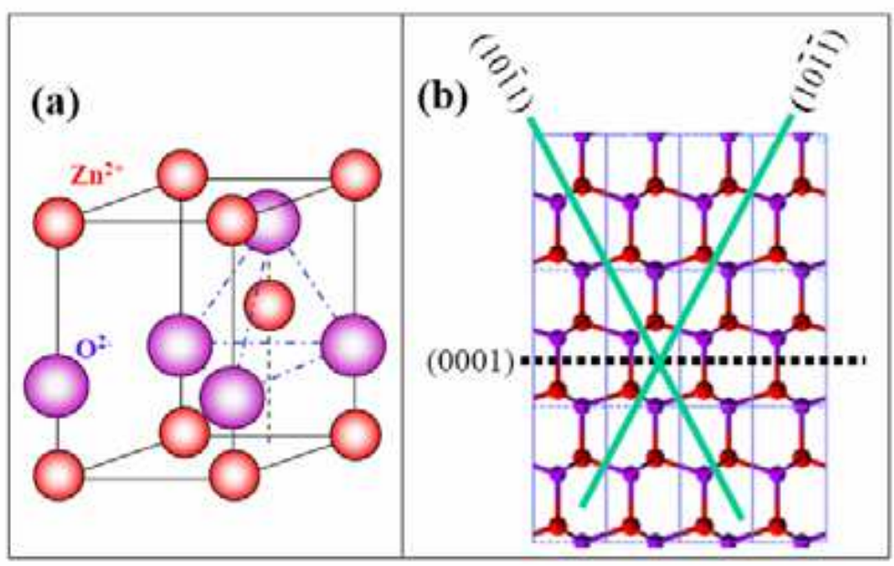

Fig. 1. (a) Wurtzite structure model of ZnO. The tetrahedral coordination of Zn-O is shown. (b) The structure model of ZnO projected along [2 $\bar{1}$ $\bar{1}$ 0], displaying the ±(0001), ± (01 $\bar{1}$ $\bar{1}$) and ± (01 $\bar{1}$ 1) polar surfaces

3. Growth of ZnO nanostructures

Growth of ZnO nanostructures has been carried out by several groups using the techniques that are still being developed for their reliability and throughput. These approaches are listed in three broad categories. These include:

1. Vapor Phase Deposition Technique (Solid-Vapor Process) [10]
2. Chemical Synthesis Method [10]
3. Induction Heating Method [11]
4. Metal-Organic Chemical Vapor Deposition (MOCVD) [12,13]

There are several processing parameters such as temperature, pressure, carrier gas (including gas species and its flow rate), substrate and evaporation period, which can be controlled and need to be selected properly before and/or during the thermal vaporization [10]. The source temperature selection mainly depends on the volatility of the source material(s). Usually, it is slightly lower than the melting point of the source material. The pressure is determined according to the evaporation rate or vapor pressure of the source material(s). The schematic representation of the Vapor Phase Deposition technique is shown in figure 2.

The substrate temperature usually drops with the distance of its location from the position of the source material(s). The local temperature determines the type of product that will be obtained. It is also noted that the thermal evaporation process is very sensitive to the concentration of oxygen in the growth system. Oxygen influences not only the volatility of

the source material(s) and the stoichiometry of the vapor phase, but also the formation of the product(s).

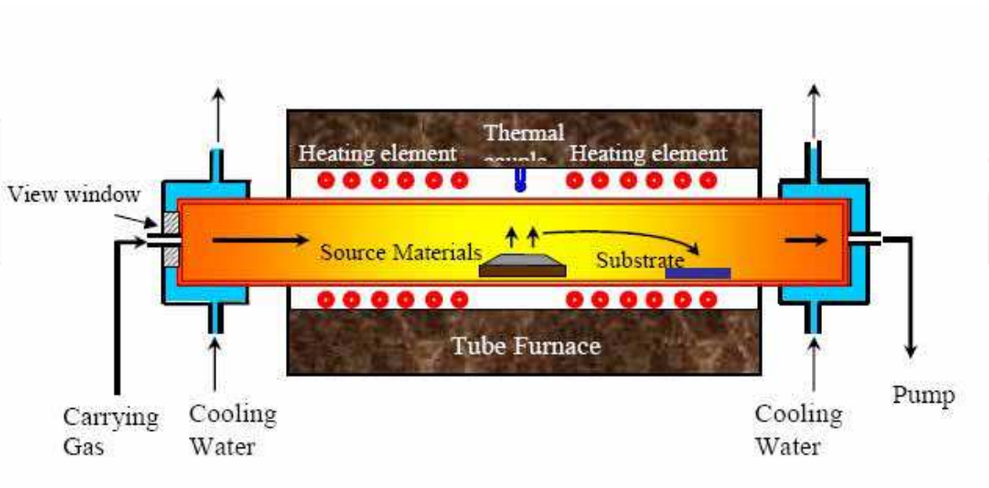

Fig. 2. A schematic diagram of the experimental apparatus for growth of oxides nanostructures by the solid–vapor phase process [Wang et al; Ref 10]

The Second Growth approach for ZnO nanowires uses the chemical synthesis method [10]. This is a hydrothermal method, where the growth procedure for growth of ZnO nanowires is as follows:1). Suspend the surface modified substrate in a Pyrex glass bottle filled with an equal molar aqueous solution of zinc nitrate hydrate (Zn(NO3)2.6H2O) and hexamethylenetetramine (C6H12N4) at temperatures between 60-90 C. 2). The temperature, PH, solution concentration, reaction time (a range of 1-72 hours) and substrate surface status were optimized for growing Nanowire arrays with controlled dimensions and orientation. 3). after completion of the reaction, the substrates were removed from the solution, and rinsed by de-ionized water, and dried in air at 65 C.

The third approach uses the inductive heating assisted fast synthesis of ZnO nanowires using ZnO/graphite solid source powder in a room temperature environment [13]. The internal heat generation induced by the alternating magnetic field at the synthesis specimen enables the fast temperature transition for ZnO nanowire growth, with a synthesis time less than 5 min compared to conventional methods. Furthermore, this demonstration illustrates the feasibility of a simple and fast nanoscale synthesis using inductive heating for nanomaterials synthesis [13].

Figure 3a shows the schematic illustration for the ZnO nanowire synthesis setup. The synthesis specimen is placed inside a quartz tube underneath the center of an eight-turn inductive coil with a pitch of 3.25 mm and an inner/outer diameter of 12.7/ 19.2 mm. The distance between the coil base and the synthesis specimen is - 6 mm.

The cross sectional view of the synthesis specimen, including a nickel coated heating chip, source powder, and growth chip inside a ceramic boat, is shown in Figure 3 b. When an alternating current is applied in the coil, an alternating magnetic field is generated, which induces eddy currents in the nickel layer and provides rapid Joule heating for nanowire synthesis. Analytically, one can derive each coil's magnetic field intensity generated at any point with a scalar distance of *d* with respect to the coil loop center from Biot-Savart's law [Lin et al 2007; Ref 11].

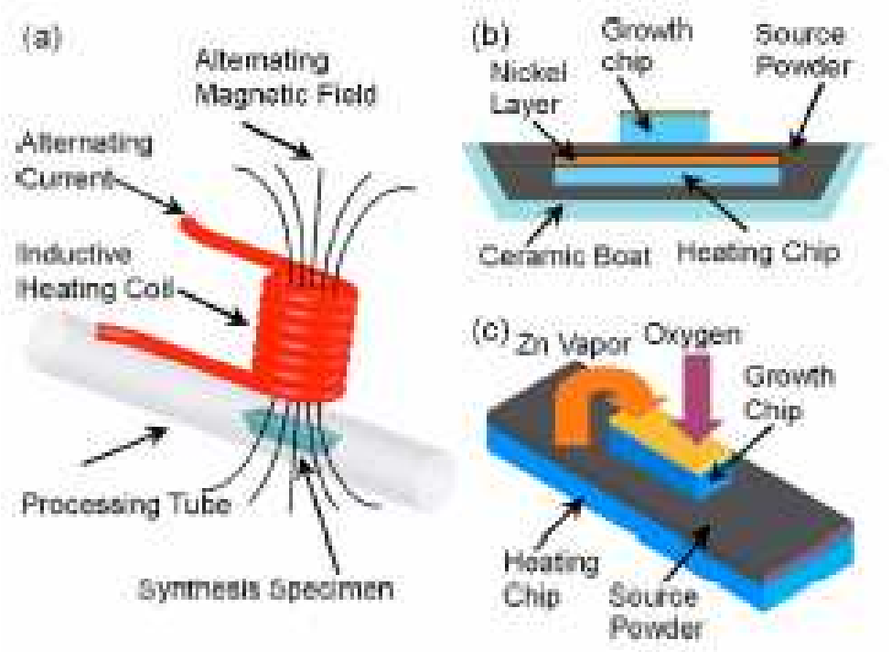

Fig. 3. Schematic illustration for ZnO nanowire synthesis setup using induction heating method (a). Cross sectional view of the synthesis specimen consisting of a heating chip, source powder, and growth chips inside a ceramic boat (b). Three-dimensional sketch of the heating chip/source powder/growth (c) [Lin et.al; Ref 11]

Several groups are have used Metal-Organic Chemical Vapor Deposition (MOCVD) successfully to grow ZnO nanostructures and have shown good results [12, 13]. Further work is underway to develop this technology for oriented ZnO nanowires for optoelectronic applications.

4. Oriented nanostructures growth

For the first two growth approaches, selectively patterned substrates have been used to control the density and selectivity of the aligned growth. The patterned materials can be catalysts (Au, Ni, etc.). The patternings methods are Electron-beam Lithography and Focused ion beam Microscopy.

Figure 4 presents a standard process for E-beam lithography. First step is to spin-coat E-beam resist PMMA of desired thickness layer on the substrate, and then using electron beam to selectively expose the patterned area of PMMA coating. Next step is to develop the exposed pattern using MIBK solution. After this step, the PMMA coating on the Si substrate is left with a pattern, which is subsequently filled by metal deposition, and the remaining PMMA can be lifted off in acetone.

This patterned substrate can be used for growth of ZnO nanowires. They are currently developing the lift-off process to fabricate the substrates. Once the process is refined on Silicon substrates, it can be further implemented on other substrates [10].

Figure 5 presents Au-pattern on Si substrate. We have recently achieved the Au-pattern using E-beam lithography. The patterned gold dot array is 2 um in diameter, 2 um in spacing, and 200 nm in height.

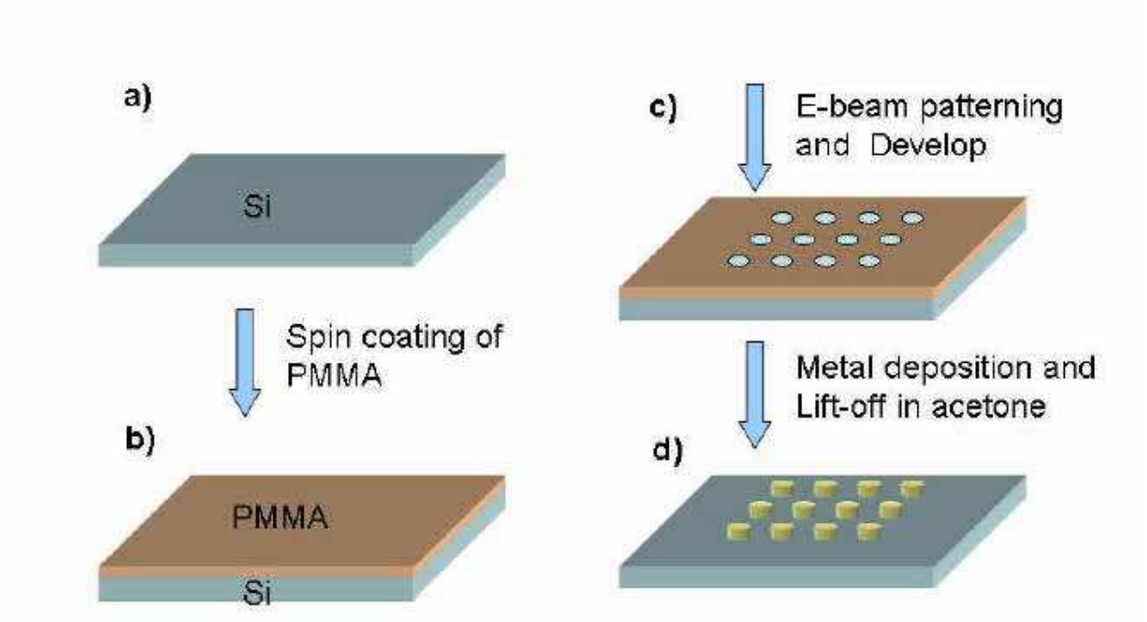

Fig. 4. E-beam Lithography Process Flow for growth of ZnO Nanowires [Wang et al; Ref 10]

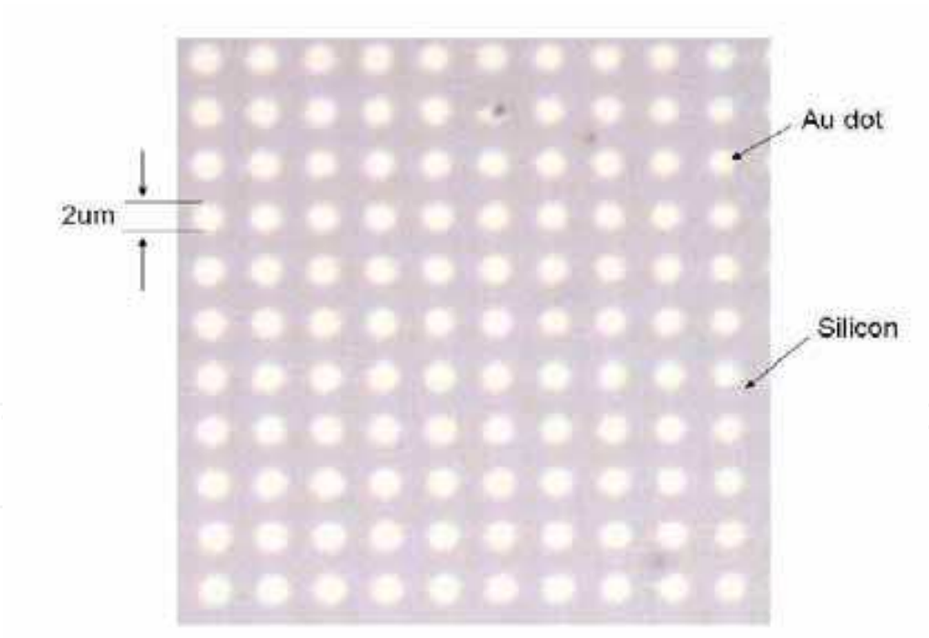

Fig. 5. Au Pattern on Silicon substrate with 20 micron size [Wang et al; Ref 10]

The hydrothermal synthesis method has been very successful in terms of synthesizing large scale nanowires arrays on Silicon substrates. As shown in figure 6a is a side view SEM image of the as grown ZnO nanowires arrays on Au-coated Si substrate, the alignment is very good. The zoom-in image in the inset displayed the dimensions of the grown nanowire, ~200 nm in diameter, ~ 5 um in lengths.

Figure 6b shows the top view of aligned nanowire arrays; the top-right inset enlarged picture clearly illustrated the hexagonal cross-section of the nanowires. The bottom-right CCD image is showing a 2-inch diameter sized area of nanowires arrays grown on an Au-coated substrate.

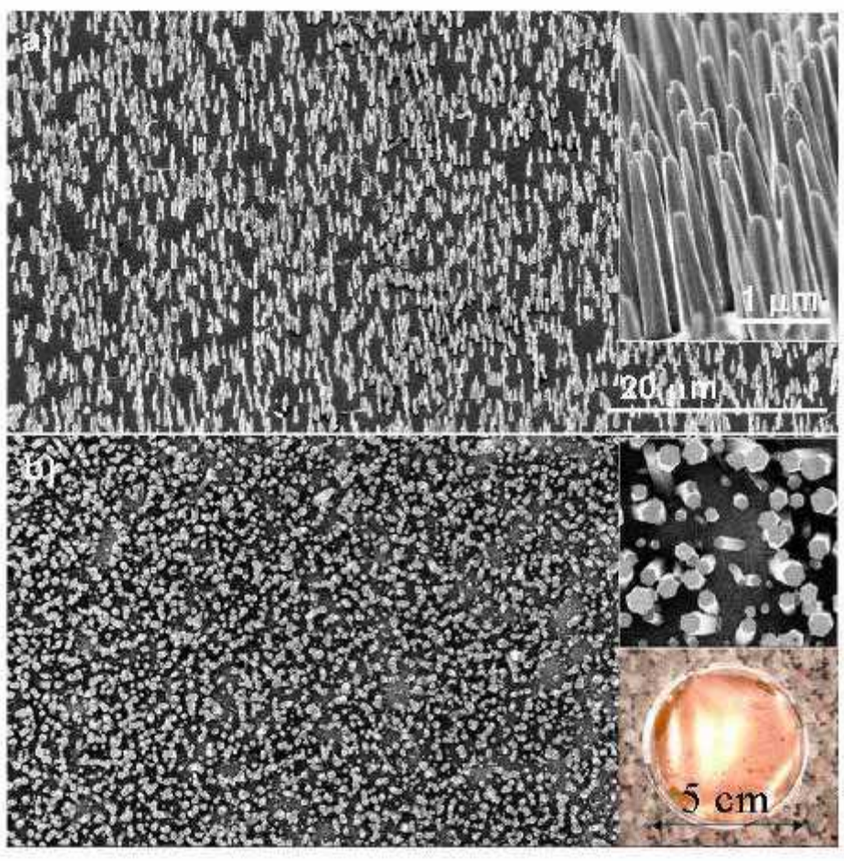

Fig. 6. ZnO Nanowires grown on Silicon Substrate [Wang et al; Ref 10]

Besides Au, they have also evaluated the ZnO seeds for promoting growth of ZnO nanowires using hydrothermal synthesis. As shown in figure 6a, a low-magnification SEM image showing the growth of ZnO nanowires on ZnO seeds coated (30 nm in thickness) PMMA film. The wavy feature is due to the non-uniform PMMA coating surface. The enlarged top view was revealed in figure 6b, witnessing the randomly grown nanowires with sharp tips ~20 nm in diameter. The EDS analysis in figures 6c-d revealed the main composition of ZnO with some impurities. They have identified the impurity to be Chromium (Figure 6d).

Density controls of nanowires growth are also being studied as an important parameter for the UV detector and Sensor application. As shown in figure 7, a typical dispersive nanowires array on Au-coated Si substrate. The wire diameter is about 1-2 um (figure 7 b), the length can be as long as 30 um, and the spacing in between nanowires are ~5-15 um. Figure 7c revealed the additional growth of nanoscale ZnO dots on the Si substrate corresponding to the densely distributed nanodots in figure 7b, which might be the seeds (nuclei) of ZnO nanowires growth.

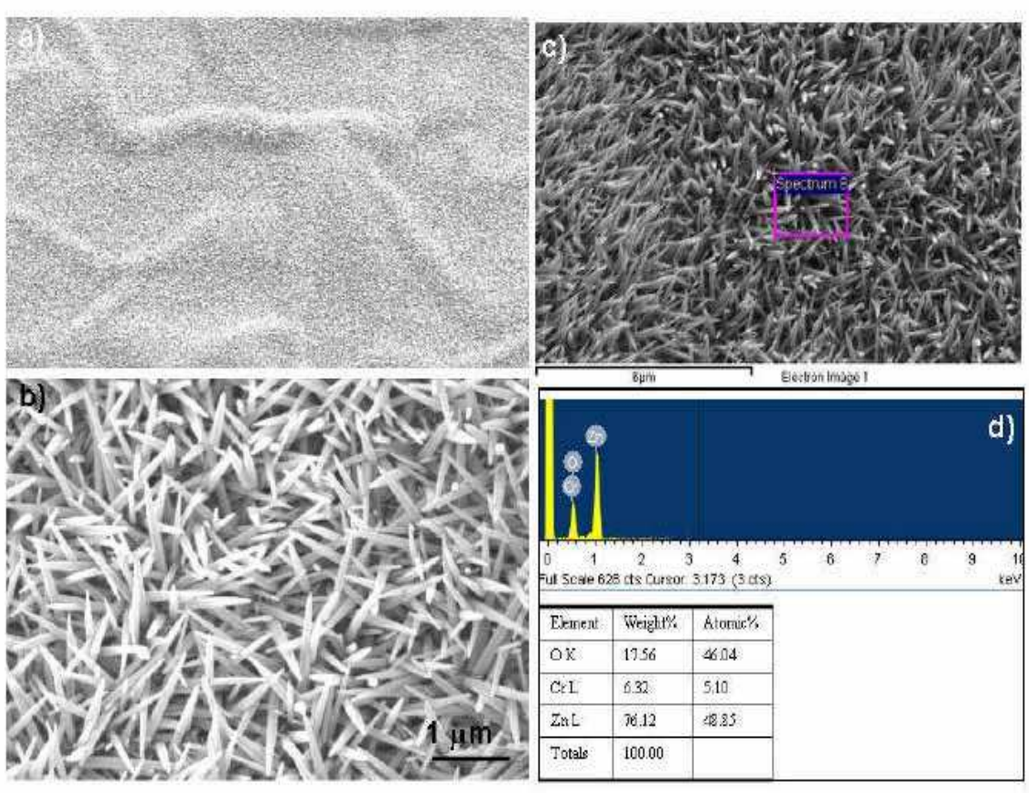

Fig. 7. ZnO nanowire growth on ZnO coated substrates [Wang et al; Ref 10]

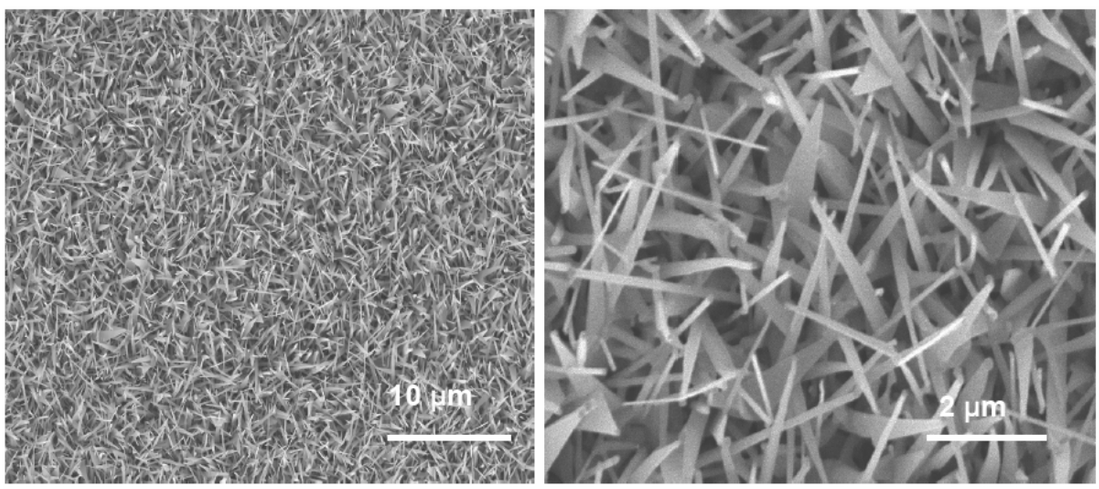

Fig. 8. ZnO nanowires grown on SiC (0001) substrates with 2 nm Au at 960 C [Wang et al; Ref 10]

They have also evaluated growth of ZnO nanowires on SiC substrates. SiC being a wide bandgap semiconductor can be used for active device fabrication. For this effort, we have used SiC (0001) substrates. We have used thermal evaporation method using ZnO and C as source material. Au, 2-4 nm thick was used as a catalyst for the growth. We also used Argon

and Oxygen as the carrier gases. Figure 8 presents the ZnO nanowires and nanosheets on SiC (0001) coated with 2 nm gold. The growth was carried out at 960 C, using Argon and Oxygen. The growth was carried out for 30 minutes.
The results in figures 8 show their attempts to grow the ZnO nanowires. The process is still being optimized for oriented growth with different growth temperatures and gas flow along with various catalysts. These nanowires show that high density growth of ZnO nanowires is quite feasible and need further growth optimization for oriented growth. Figure 9 presents the TEM characterization of ZnO nanowires grown on SiC (0001) substrate with Au catalyst. This can open a variety of device configurations for optical and other applications using ZnO nanowires.

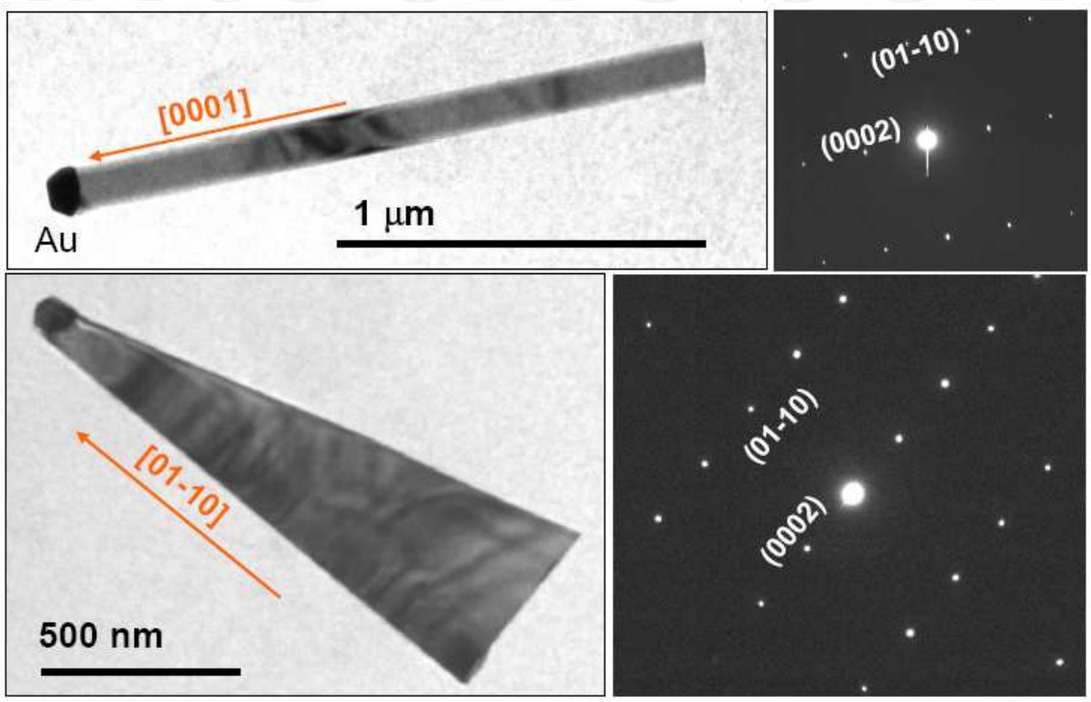

Fig. 9. TEM characterization of ZnO nanowires grown on SiC (0001) substrates shown in figure 8.The orientation of ZnO nanowires with two orientations are illustrated [Wang et al; Ref 10]

Their work has shown that Sn can also be an effective catalyst for growing ZnO nanorods [14]. Using the epitaxial growth of ZnO nanorods on ZnO crystal, aligned nanorods have been grown as shown in figure 10. In this case, the growth direction of the nanorods is led by the Sn catalyst and the epitaxial orientation is defined by the substrate that determines the aligned growth. The nanorods are also aligned in orientation because they tend to take the least mismatch orientation on the substrate, to reduce the interface mismatch energy.
The choice of substrate is important for the epitaxial growth. One must consider the crystallographic structure as well as the surfaces to be used for the growth. We have found recently that the atomic termination and charge status of the substrate can strongly affect the morphology of the grown nanorods [14]. The nanorods growing out of Zn-terminated (0001) ZnO substrates are very different from those grown out of the oxygen-terminated $(000\bar{1})$ ZnO substrates although the same type of Sn catalyst was used.

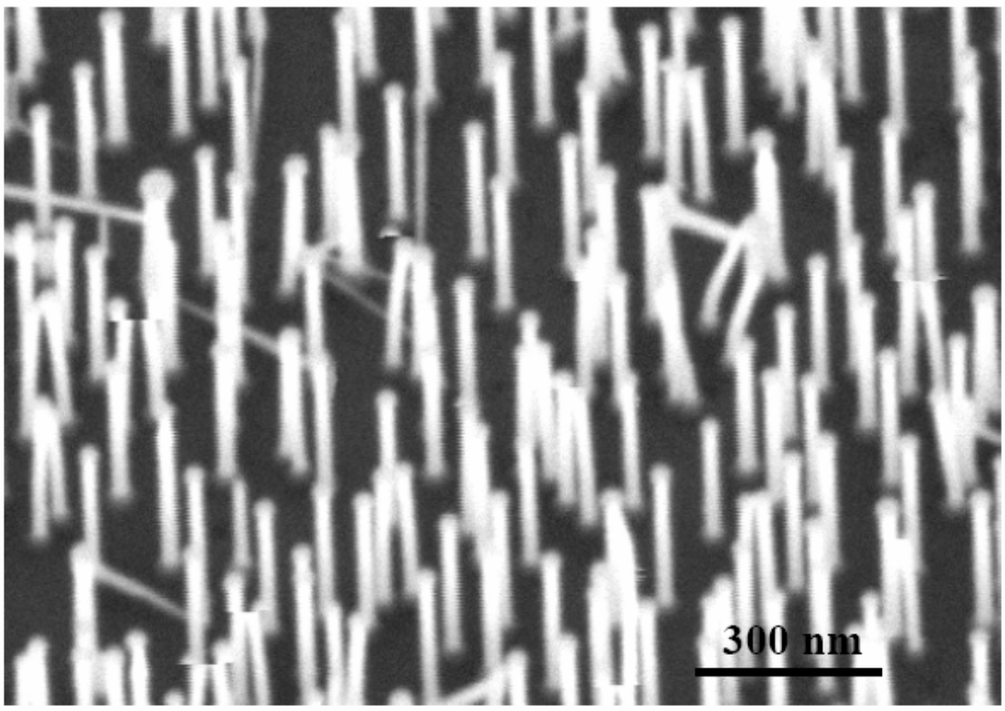

Fig. 10. Aligned ZnO nanorods/nanowires epitaxially grown on ZnO substrate using Sn as a catalyst [Gao et. al; Ref 15]

5. ZnO nanowires properties and optical device applications

ZnO exhibits a direct band-gap of 3.37 eV at room temperature with large exciton energy of 60 meV. The strong exciton binding energy, which is much larger than that of GaN (25 meV), and the thermal energy at room temperature (26 meV) can ensure an efficient exciton emission at room temperature under low excitation energy. As a consequence, ZnO is recognized as a promising photonic material in the blue–UV region.

Single-crystalline ZnO nanowires have been synthesized using high temperature VLS growth methods discussed above [10, 16]. Room temperature UV lasing in ZnO nanowires has been demonstrated [17]. PL spectra of the ZnO nanorods were measured with a fluorescence spectrophotometer using a Xe lamp with an excitation wavelength of 325 nm at room temperature. Figure 11 shows the PL spectrum of the ZnO nanorods with a diameter in the range 60 ± 80 nm. Three emitting bands, including a strong ultraviolet emission at around 386 nm and a very weak blue band (440 ± 480 nm) as well as an almost negligible green band (510 ± 580 nm), were observed.

The UV emission must be contributing to the near band edge emission of the wide band-gap ZnO. It has been suggested that the green band emission corresponds to the singly ionized oxygen vacancy in ZnO and results from the recombination of a photo-generated hole with the singly ionized charge state of this defect. The stronger the intensity of the green luminescence, the more singly ionized oxygen vacancies there are. Thus the almost negligible green band in figure 11 shows that there is a very low concentration of oxygen vacancies in the well-aligned ZnO nanorods. The observation of blue band emission (440 ± 480 nm) of ZnO film has also been reported, using cathodoluminescence.

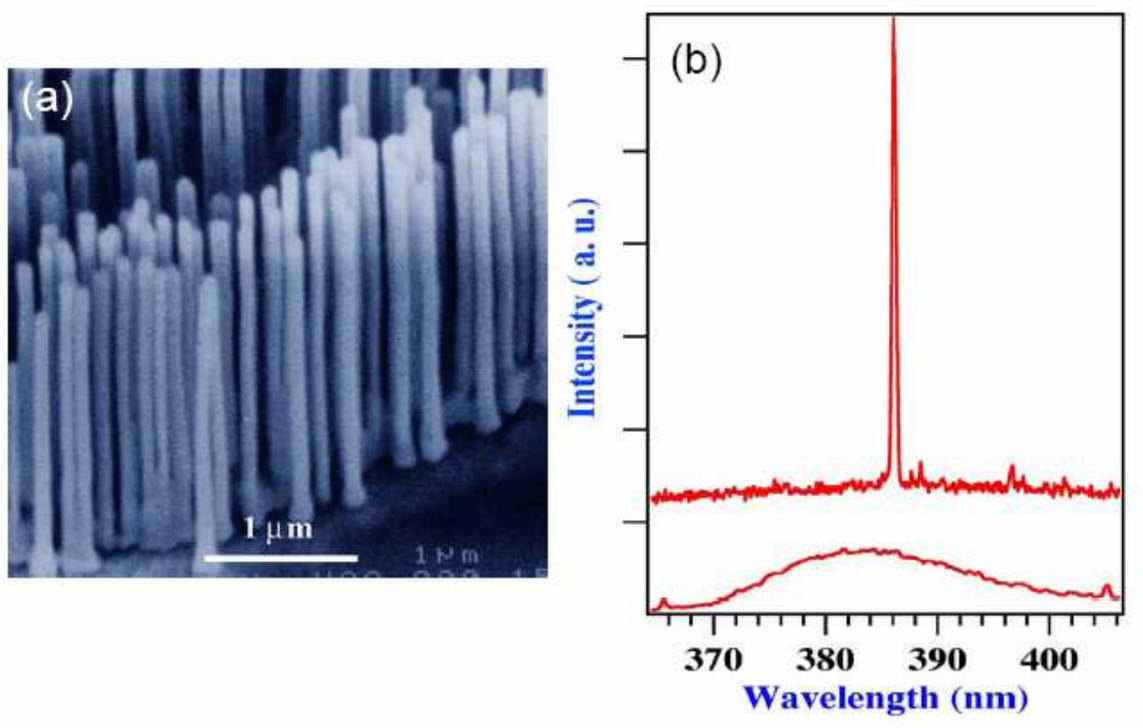

Fig. 11. (a) An SEM image of aligned ZnO nanowire arrays grown on sapphire substrate coated with a 3 nm thick layer of Au. (b) Emission spectra from nanowire arrays at pump powers of 20 and 100 kW cm -2. The spectra are offset for easy comparison. Stimulated emission from the nanowires was collected in the direction along the nanowire end-plane normal (the symmetric axis) with a monochromator. All experiments were carried out at room temperature [P.D, Yang et al.; Ref 17]

6. ZnO nanowire field effect transistor

Field effect transistors have been fabricated using individual nanobelts [18]. Large bundles of ZnO nanobelts were dispersed in ethanol by ultrasonication until mostly individual nanobelts were isolated. These ethanol dispersions were dried onto a SiO_2/Si substrate for imaging by non-contact mode atomic force microscopy (AFM). Field effect transistors were fabricated by depositing dispersed ZnO nanobelts on predefined gold electrode arrays. The SiO_2 gate dielectric thickness was 120 nm and the back gate electrode was fabricated by evaporation of gold on the Si (p+) side of the substrate.

In addition, in both fabrication schemes, the electrode arrays were variably spaced. They included electrode gaps as small as 100 nm and as large as 6 μ m. An AFM image of the field effect transistor (FET) and a schematic diagram are shown in figure 12. The principle of this device is that controlling the gate voltage would control the current flowing from the source to the drain.

By forming metal electrode/nanostructure electrical contacts and capacitively coupling the nanostructure to a nearby gate electrode, an FET is produced using a nanobelt that allows the exploration of new aspects of the physical and chemical properties of the nanostructures [19, 20. 21].

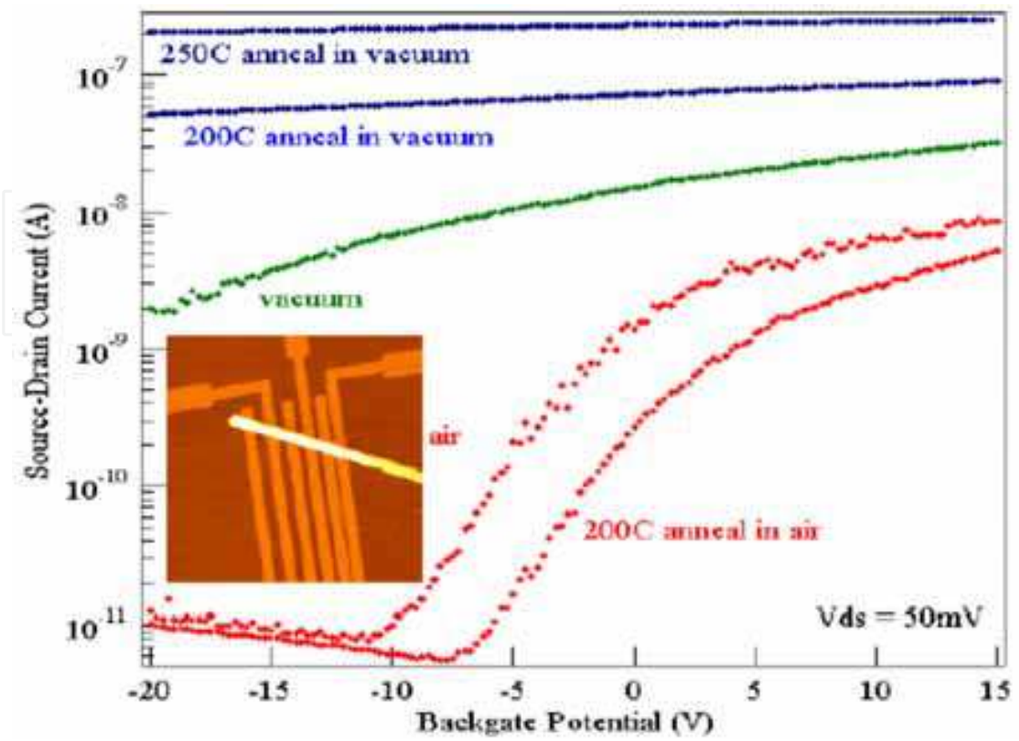

Fig. 12. ZnO nanobelt FET. Source–drain current versus gate bias for a SnO_2 FET after various treatments measured in this order: air, vacuum, 200 C vacuum anneal, 250 C vacuum anneal, 200 C air anneal. The inset shows a field effect transistor (FET) device made using a single nanobelt. [Wang et al; Ref 22]

The alternative way of contacting the nanobelts by simply depositing them on top of pre-fabricated gold electrodes led to very resistive contacts. A typical ZnO field effect transistor showed a gate threshold voltage of −15 V, a switching ratio of nearly 100 and a peak conductivity of $1.25 \times 10^{-3}\ \Omega\ cm^{-1}$. A completely analogous behavior has been observed in the case of carbon nanotubes deposited on top of Au electrodes or covered by Ti electrodes [22].

7. UV photoconductivity measurements on ZnO nanostructures

Ultraviolet light irradiation of the nanobelt diode of ZnO in air is observed to result in a significant increase of the conductivity [Figure. 13]. Light with a wavelength of 350 nm (E_λ = 3.54eV) was used, exceeding the direct band-gap of ZnO. The increase in the conductivity results from both photo- generation of electron-hole pairs as well as doping by UV light-induced surface desorption. These processes could be observed by introducing a shutter between the light source and the ZnO nanobelt so that the flux of UV photons could be turned 'ON' and 'OFF'.

The unique geometrical shape of nanobelts is ideal for field emission. MoO_3 nanobelts have been shown to exhibit superior performance. The work function at the tips of individual ZnO nanobelts has been measured by a novel technique [23].

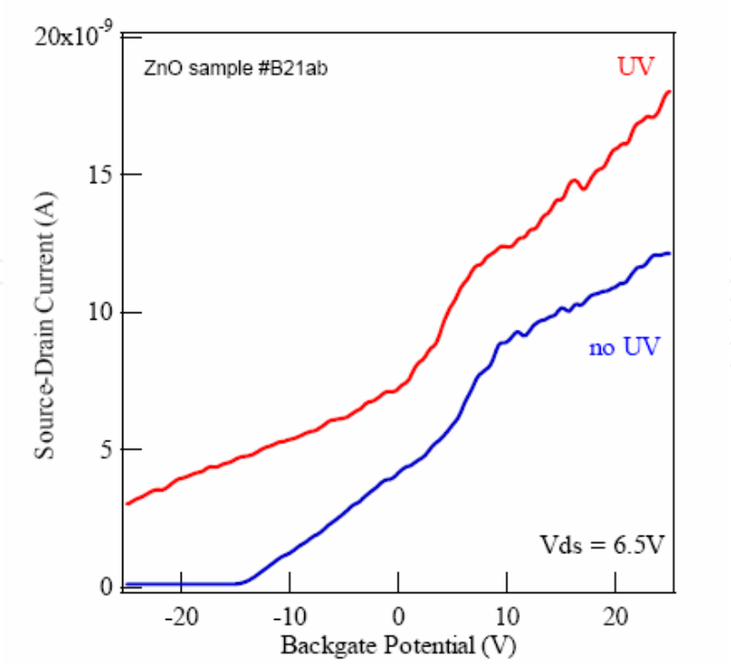

Fig. 13. Source-drain current measured from a ZnO nanobelt FET, showing a strong dependence on UV illumination [Wang et al; Ref 22]

8. ZnO nanowire piezoelectric nanogenerator

Wireless devices may allow in-situ, real-time biomedical monitoring and detection, but such devices still requires a power source. Ideally, such devices should be self-powered rather use a battery. The body provides numerous potential power sources - mechanical energy, vibrational energy, chemical energy (glucose), and hydraulic energy, but the challenge is their efficient conversion into electric energy. If accomplished on the nanoscale such power sources could have greatly reduced the size of the integrated nanosystems for optoelectronics [24], biosensors [25], resonators [26] and more. They have demonstrated an approach of converting mechanical energy into electric power using aligned ZnO NWs [27]. Their study is based on aligned ZnO NWs grown on c-plane oriented -Al_2O_3 substrate covered by a layer of ZnO film (Figure 14 a). The measurements were performed by AFM using a Si tip coated with Pt film. In the AFM contact mode, a constant normal force of 5 nN was maintained between the tip and sample surface. The tip scanned over the top of the ZnO NW, and the tip's height was adjusted according to the surface morphology and local contacting force. The output voltage across an outside load of resistance R_L = 500 MΩ was continuously monitored as the tip scans over the NWs (note the defined polarity of the voltage signal) (Figure 14b). No external voltage was applied in any stage of the experiment. Experimentally, both the topography (feedback signal from the scanner) and the corresponding output voltage (V_L) images across the load were recorded simultaneously when the AFM tip was scanned over the aligned NW arrays. In the voltage output image, many sharp output peaks (like discharge peaks) were observed, which are typically about 4 to 50 times higher than the noise level (Figure 14c). The location of the voltage peak is directly registered at the site of the NW.

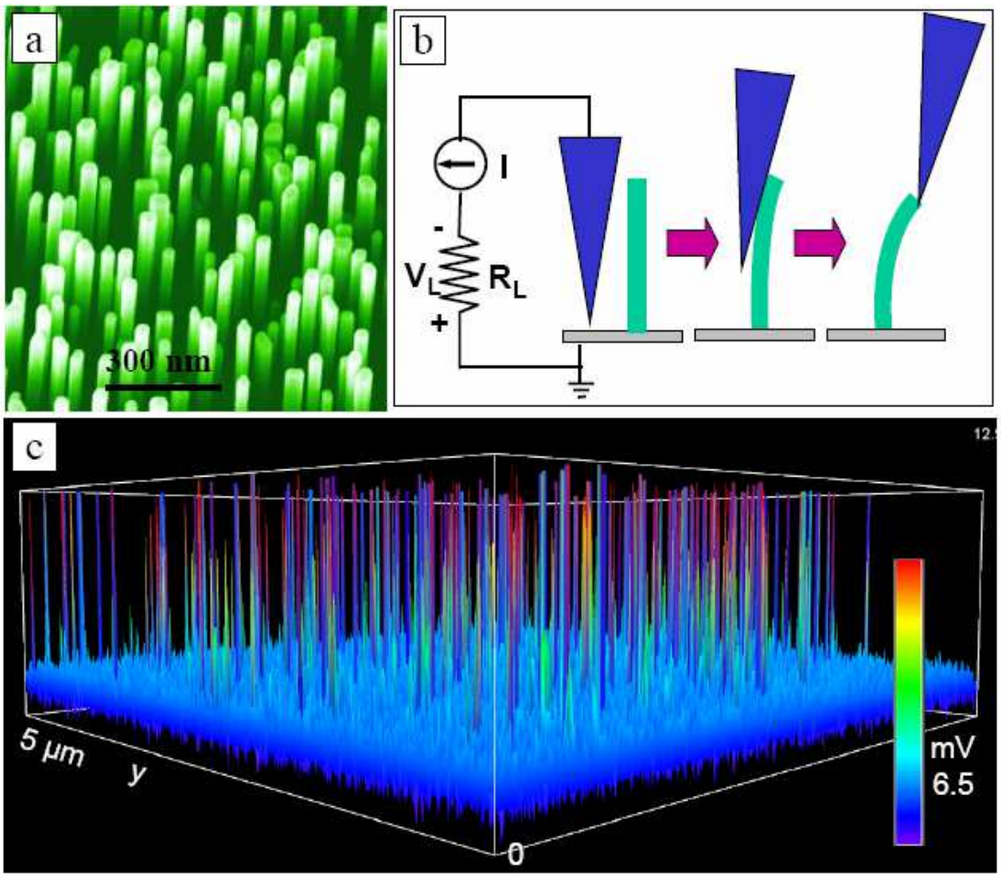

Fig. 14. (a) SEM images of aligned ZnO NWs grown on α-Al_2O_3 substrate. (b) Experimental set up and procedures for generating electricity by deforming a piezoelectric NW using a conductive AFM tip. The root of the NW is grounded, and an external load of R_L = 500 MΩ is applied, which is much larger than the inner resistance R_I of the NW. The AFM scans across the NW arrays in contact mode. (c) Output voltage image of the NW arrays when the AFM tip scans across the NW arrays. The discharging process is so quick that each discharge event is characterized by only a couple of data points. This gives a difficulty of displaying the data by rainbow color. [Wang et al; Ref 27]

The physical principle for creating, separating and preserving the PZ charges in the NW is a coupling of piezoelectric (PZ) and semiconducting properties [27, 28]. For a vertical, straight ZnO NW (Figures 15a), the deflection of the NW by AFM tip creates a strain field, with the outer surface being stretched (positive strain) and inner surface compressed (negative strain) (Figures 15b).

An electric field E_z along the NW (z direction) is then created inside the NW volume through the PZ effect, $E_z = \ _z /d$, where d is the PZ coefficient[29] along the NW direction that is normally the positive c-axis of ZnO, with the Zn atomic layer being the front terminating layer [30]. The PZ field direction is closely parallel to the z-axis (NW direction) at the outer surface and anti-parallel to the z-axis at the inner surface (Figures 15c). Under the first-order approximation, across the width of the NW at the top end, the electric potential distribution from the compressed to the stretched side surface is approximately between V_s^- (negative) to V_s^+ (positive).

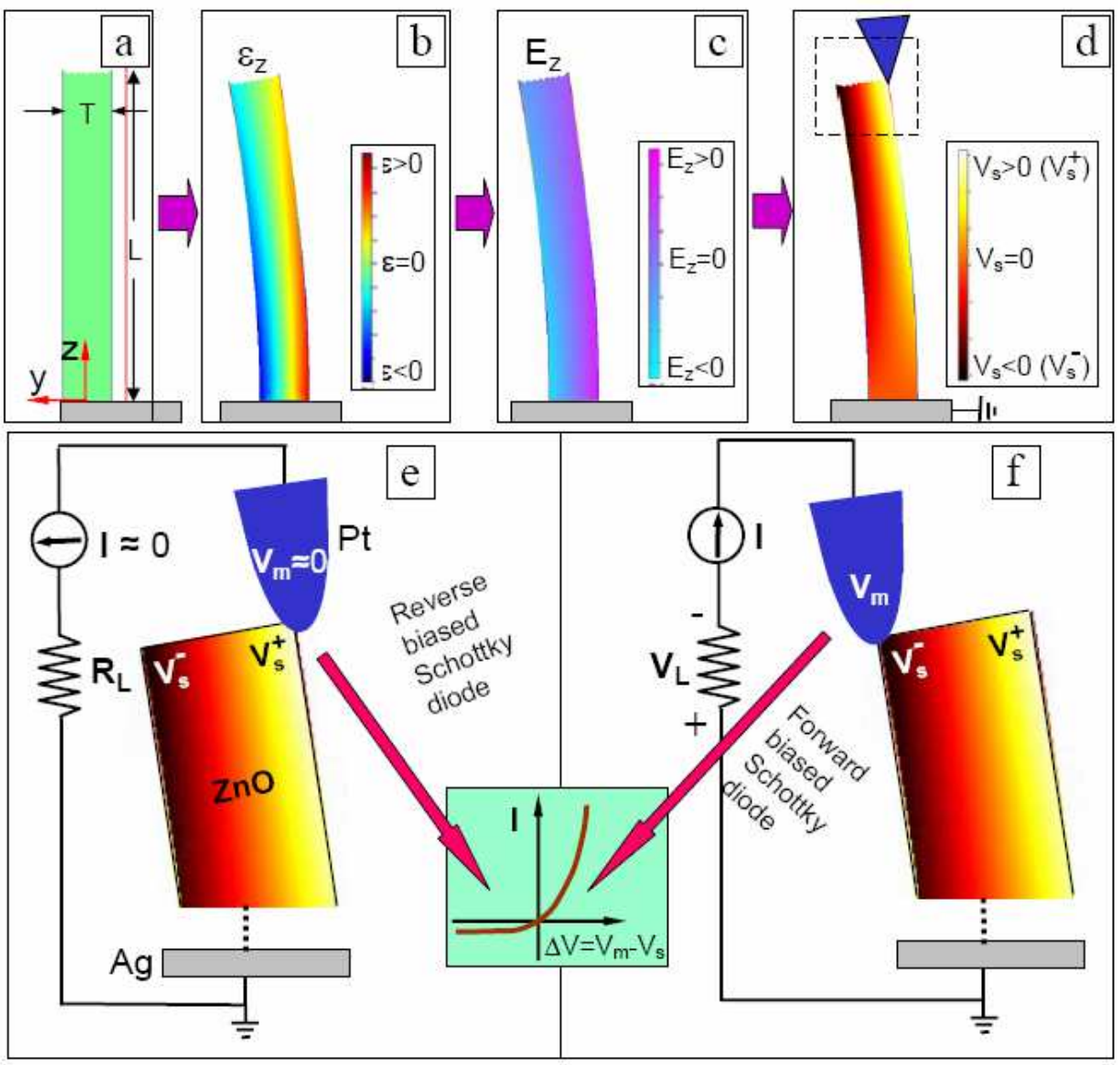

Fig. 15. Physical principle of the observed power generation process of a piezoelectric ZnO NW, showing a unique coupling of piezoelectric and semiconducting properties in this metal-semiconductor Schottky barrier governed transport process. (a) Schematic definition of a NW and the coordination system. (b) Longitudinal strain ε_z distribution in the NW after being deflected by an AFM tip from the side. The data was simulated by FEMLAB for a ZnO NW of length 1 μm, aspect ratio of 10. (c) The corresponding longitudinal piezoelectric induced electric field E_z distribution in the NW. (d) Potential distribution in the NW as a result of piezoelectric effect. The dashed box indicates the area to be examined in details in (e, f). (e, f) Metal and semiconductor contacts between the AFM tip and the semiconductor ZnO NW at two reversed local contact potentials (positive and negative), showing reverse and forward biased Schottky rectifying behavior, respectively (see text). It is this oppositely biased Schottky barrier across the NW makes it possible to preserve the piezoelectric charges and later produce the discharge output. Inset is a typical I-V characteristic of a metal-semiconductor (n-type) Schottky barrier. The process in (e) is built up the potential; the process in (f) is to discharge the potential. [Wang et al; Ref 27, 28]

The electrode at the base of the NW is grounded. Note the V_s^+ and V_s^- are the voltages produced by PZ effect, respectively. The potential is created by the relative displacement of the Zn^{2+} cations with respect to the O^{2-} anions due to PZ effect in the wurtzite crystal structure; thus, these ionic charges cannot freely move and cannot recombine without releasing the strain (Figures 15d). The potential difference is maintained as long as the deformation is in place and no foreign free charges (such as from the metal contacts) are injected.

We now consider the discharge process. In the first step, the AFM conductive tip that induces the deformation is in contact with the stretched surface of positive potential V_s^+ (Figure 15d and e). The Pt metal tip has a potential of nearly zero, $V_m = 0$, so the metal tip - ZnO interface is negatively biased for $V = V_m - V_s^+ < 0$. With consideration the n-type semiconductor characteristic of the as-synthesized ZnO NWs, the Pt metal- ZnO semiconductor (M-S) interface in this case is a reverse-biased Schottky diode (Fig. 40e), and little current flows across the interface. In the second step, when the AFM tip is in contact with the compressed side of the NW (Figure 415f), the metal tip - ZnO interface is positively biased for $V = V_L = V_m - V_s^- > 0$.

The M-S interface in this case is a positively biased Schottky diode, and it produces a sudden increase in the output electric current. The current is the result of V driven flow of electrons from the semiconductor ZnO NW to the metal tip. The flow of the free electrons from the loop through the NW to the tip will neutralize the ionic charges distributed in the volume of the NW and thus reduce the magnitudes of the potential V_s^- and V_s^+.

The principle and technology demonstrated here have the potential of converting mechanical movement energy (such as body movement, muscle stretching, blood pressure), vibration energy (such as acoustic/ultrasonic wave) [74], and hydraulic energy (such as flow of body fluid, blood flow, contraction of blood vessel, dynamic fluid in nature) into electric energy that may be sufficient for self-powering nanodevices and nanosystems.

The technology could have important applications in wireless self-powered nanodevices by harvesting energy from the environment. It also provides a method for indirectly charging of a battery. It is also possible to fabricate large-power output electric generator by using arrays of ZnO wires/belts, which can be grown on substrates such as metal foils, flexible organic plastic substrates [31], ceramic substrates (such as alumina) and compound semiconductors (such as GaN and AlN). The nano-generator could be the basis for exploring new self-powering technology for in-situ, real-time and implantable Biosensing, biomedical monitoring and biodetection. It could have the potential of solving key energy requirement for remote sensing and actuating.

9. Ultrasonic wave driven nanogenerators using ZnO nanowires

For practical applications, we must make an innovative design to drastically improve the performance of the Nanogenerators in following aspects. First, we must eliminate the use of AFM for making the mechanical deformation of the NWs so that the power generation can be achieved by an adaptable, mobile and cost-effective approach over a larger scale. Secondly, all of the NWs are required to generate electricity simultaneously and continuously, and all the electricity can be effectively collected and output.

Finally, the energy to be converted into electricity has to be provided in a form of wave/vibration from the environment, so the nanogenerator can operate "independently" and wirelessly. An innovative approach has been developed by Wang's group to use ultrasonic waves to drive a nanogenerator built from an array of vertically aligned ZnO NWs [32, 33]. The design is novel and cost-effective and has the potential to meet the requirements outlined above. The approach is the basic platform for optimizing and improving the performance of the nanogenerator for its applications in nanotechnology.

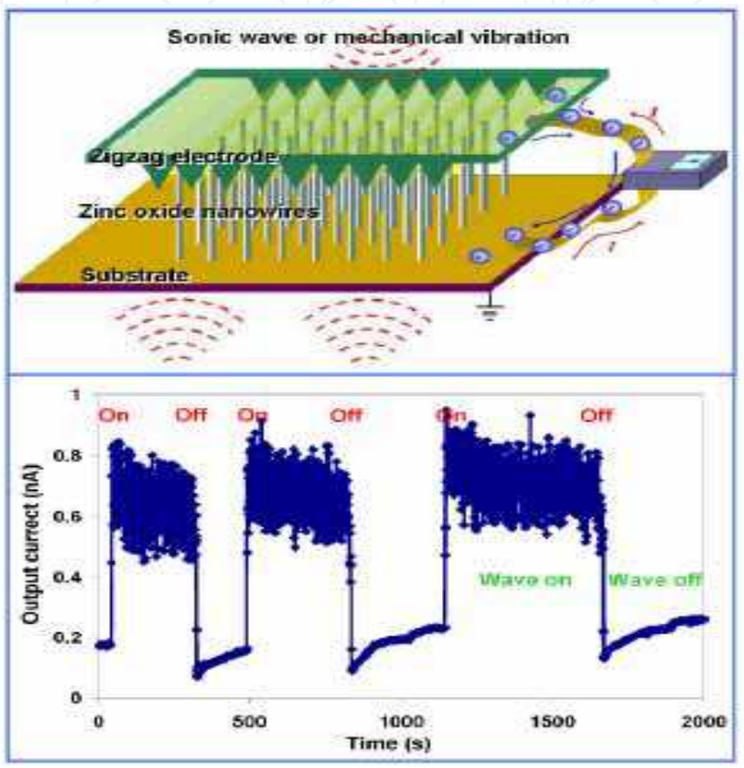

Fig. 16. Schematic diagram showing the direct current nanogenerator built using aligned ZnO nanowire arrays with a Zigzag top electrode. The nanogenerator is driven by an external ultrasonic wave or mechanical vibration and the output current is continuous. The lower plot is the output from a nanogenerator when the ultrasonic wave was on and off. The nanowire that simultaneously contributed to the DC current was estimated about 500

The experimental set up is schematically shown in Figure 16, in which an array of aligned ZnO NWs is covered by a zigzag Si electrode coated with Pt. The Pt coating is not only for enhancing the conductivity of the electrode but also for creating a Schottky contact at the interface with ZnO. The NWs were grown on either GaN substrates, which served as a common electrode for directly connecting with an external circuit. The asymmetric piezoelectric-potential across the width of a ZnO NW and the Schottky contact between the metal electrode and the NW are the two key processes for creating, separating, preserving/accumulating, and outputting the charges.

A top electrode is designed to achieve the coupling process and to replace the role played by the AFM tip, and its zigzag trenches are to act as an array of aligned AFM tips. The DC nanogenerator is driven by ultrasonic wave. Once the wave is on, about 500 nanowires

within an area of 2 mm² gives 1 nA DC current. We propose to fabricate a nanogenerator that is expected to output the electricity generated by all of the nanowires continuously.

10. Thin film and nanostructure solar cells

ZnO thin films and nanostructures are being developed for design and development of high efficiency solar cells [34, 35, 36]. The use of ZnO thin films and nanostructures in solar cells will provide an inexpensive option for large area solar cells. The Zinc oxide nanorods are attractive for photo-voltaic applications and this claim is based on their properties. Typical ZnO nanorods have a wurtzite structure with lattice spacing a = 0.32469 nm and c = 0.52069 nm [37].

Significant progress has been made in thin film solar cells that have demonstrated efficiency in excess of 30 percent for GaAs based multijunction solar cells, which are being used for space mission [39]. There are several different configurations that would allow high efficiency solar cells. More recently, there is interest in using GaN / InGaN and ZnO / MgZnO for development of high efficiency multijunction solar cells [40].

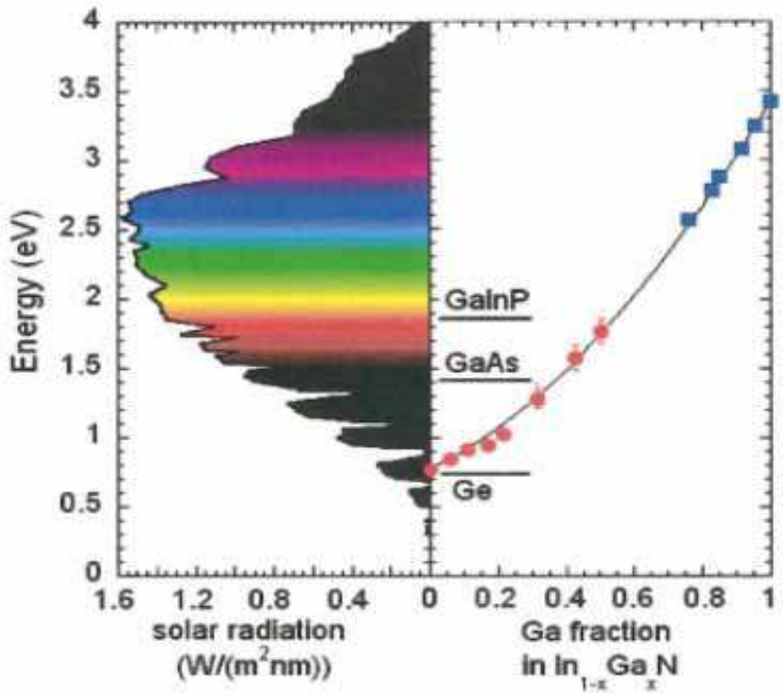

Fig. 17. Band gap energy for solar spectrum. Several material systems are being developed to provide high efficiency multijunction solar cells. These include material components Ge, GaAs and GaInP, InGaN and ZnO. [Wu et al; Reference 40]

Figure 17 presents complete solar spectrum for AM-1.5 solar cells. Different material systems can be utilized to accomplish high efficiency multijunction solar cells. Most of the multijunction solar cells have been developed for space missions where availability of high efficiency is of paramount importance and issue of radiation hardness is critical success for the space missions. There has been significant effort for development of low cost technologies that will allow high efficiency thin film solar cells for terrestrial applications.

ZnO is being explored as one of the key components for a variety of low cost thin film and nanostructure based solar cells. Recent work reported by Ganguly and his coworkers [41] has explored the use of amorphous silicon solar cells with ZnO with insertion of Germanium layers. They have shown that with insertion of a thin amorphous germanium layer at the ZnO-p-layer interface improves the cell performance and diode ideality by suppression of Oxygen and Zinc incorporation in the silicon layers. One of the advantages of ZnO is is its resistance to hydrogen plasma induced darkening and higher transmission thereby improving the solar cell efficiency.

Recent work by Peiro and his coworkers [36] at Imperial college and Manchester in UK have shown that solar cells fabricated from composites of conjugated polymers with nanostructure ZnO are of great interest for their stability, low cost and electron transport properties. ZnO polymer solar cells are promising for low temperature synthesis.

Zinc oxide (ZnO)/polymer solar cells are promising compared to other metal oxide/polymer combinations, on account of the possibility of low temperature synthesis, as well as the potential for controlling interface morphology through simple processing from solution. They have focused on the effect of surface morphology of ZnO films on photovoltaic device performance. They have successfully grown ZnO nanorods standing almost perpendicular to the electrodes on a flat, dense ZnO "backing" layer.

They have studied [36, 37] structures consisting of a conjugated polymer in contact with three different types of ZnO layer: a flat ZnO backing layer alone; ZnO nanorods on a ZnO backing layer; and ZnO nanoparticles on a ZnO backing layer. They also used scanning electron microscopy, steady state and transient absorption spectroscopy and photovoltaic device measurements to study the morphology, charge separation and recombination behavior and device performance of the three types of structures.

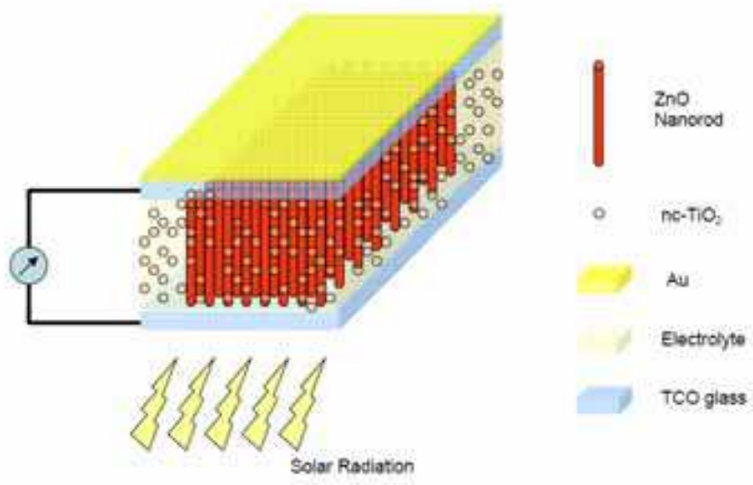

Fig. 18. Schematic diagram of ZnO based nanostructure solar cell [Sridhar et al; Ref 34]

They found that charge recombination in the structures containing vertically aligned ZnO nanorods is remarkably slow, with a half life of over 1 ms, over two orders of magnitude slower than for randomly oriented ZnO nanoparticles. A photovoltaic device based on the nanorods structure which has been treated with an ambiphilic dye before deposition of poly(3-hexyl thiophene) (P3HT) polymer shows a power conversion efficiency over four times greater than for a similar device based on the nanoparticles structure.

The best ZnO nanorods: P3HT device yields a short circuit current density of 2 mAcm-2 under AM1.5 illumination (100mWcm-2) and peak external quantum efficiency over 14%, resulting in a power conversion efficiency of 0.20%. Their effort demonstrates the potential of ZnO nanostructure based solar cells have the potential of low cost and further improvements can yield higher efficiency solar cells.

Several other groups in US, China and England [34, 36, 41, 42] are working on ZnO nanostructure solar cells. They are all trying to develop the necessary understanding for growth and characterization of ZnO nanostructures on variety of substrates.

Investigation of ZnO nanorods based solar cells is being conducted towards developing alternative, lightweight, flexible devices for commercial applications. A schematic view is shown in figure 18 .A lot of research has been done in the area of dye sensitized solar cells [37, 42] in particular, which is currently the most stable and efficient excitonic solar cell. Aligned ZnO nanorods, with their high carrier mobilities serve as the conduction pathways for the excitons. These approaches provide a glimpse of what is being done on using ZnO nanostructures fro solar cell applications. Further effort is needed in developing ZnO based solar cells that can be implemented in terrestrial applications.

11. UV atmospheric transmission model

There has been recent effort to study the atmospheric transmission models in UV, Visible and Infrared (IR) bands [43]. Modeling of atmospheric effects on transmission at UV wavelengths (250-350 nm range) was performed using MODTRAN. MODTRAN (MODerate resolution atmospheric TRANsmission) is an atmospheric radiative transfer model that may be used to determine the effects of various atmospheric layers and weather conditions on wavelength dependent free-space transmission. Six different atmospheric models were simulated: clear maritime (23 km visibility), desert extinction, drizzle (2 mm/hr), light rain (5 mm/hr), moderate rain (12.5 mm/hr), and heavy rain (25 mm/hr).

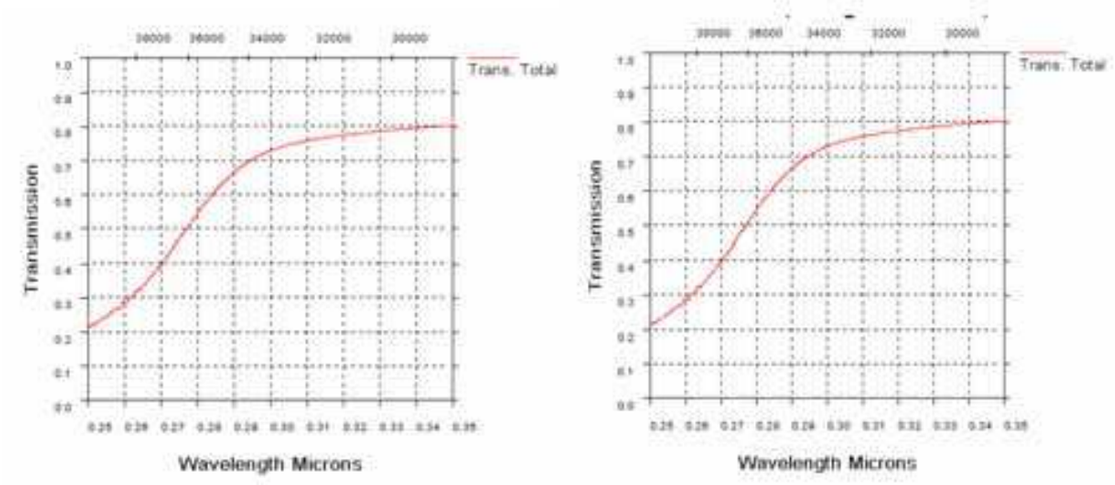

(a) (b)

Fig. 19. UV atmospheric transmission over a horizontal path in clear maritime (23 km visibility) conditions, 1 km range (19 a). UV transmission through atmosphere over a horizontal path in desert extinction conditions, 1 km range (19b)

For each of these weather conditions, UV transmission was modeled for 1 km horizontal paths through the atmosphere 5 m above the surface (Figures 1-6). In addition, slanted paths at angles of 15°, 30°, 45°, and 60° from the horizon for a distance of 10 km were simulated in clear maritime conditions (Figures 19-23) to show the relative effects of propagation though different lower atmospheric layers on attenuation. In relation to free-space optical communication networks, a 0° horizontal path would involve ground based communication extending no further than the horizon, while an upward slanted path might involve communication between a ground-based unit or sea vessel and an aircraft [43].

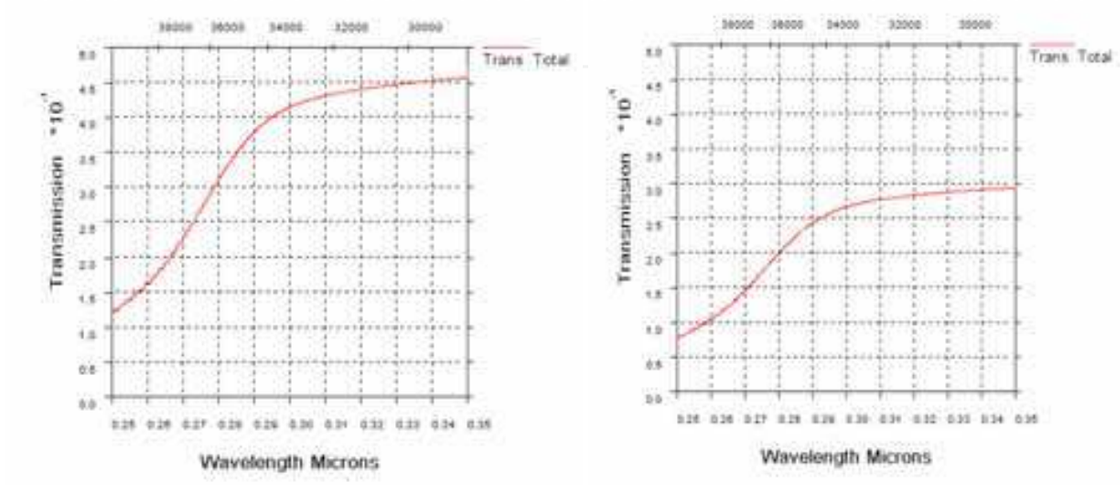

(a) (b)

Fig. 20. UV atmospheric transmission over a horizontal path in drizzle (2 mm/hr) conditions, 1 km range (20a) and UV transmission over a horizontal path in light rain (5 mm/hr) conditions, 1 km range (20b).

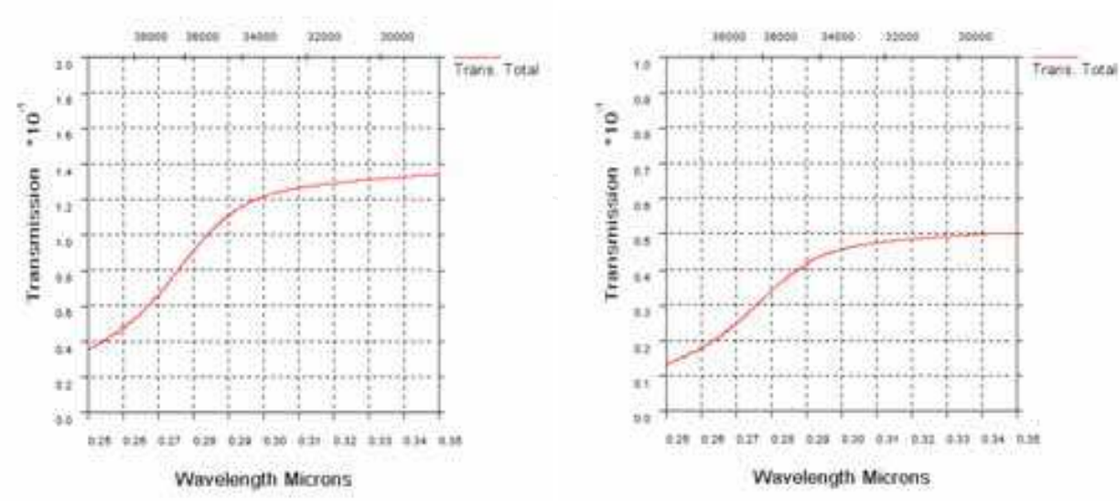

(a) (b)

Fig. 21. UV transmission through atmosphere over a horizontal path in moderate rain (12.5 mm/hr) conditions, 1 km range (21a). UV transmission over a horizontal path in heavy rain (25 mm/hr) conditions, 1 km range (21b)

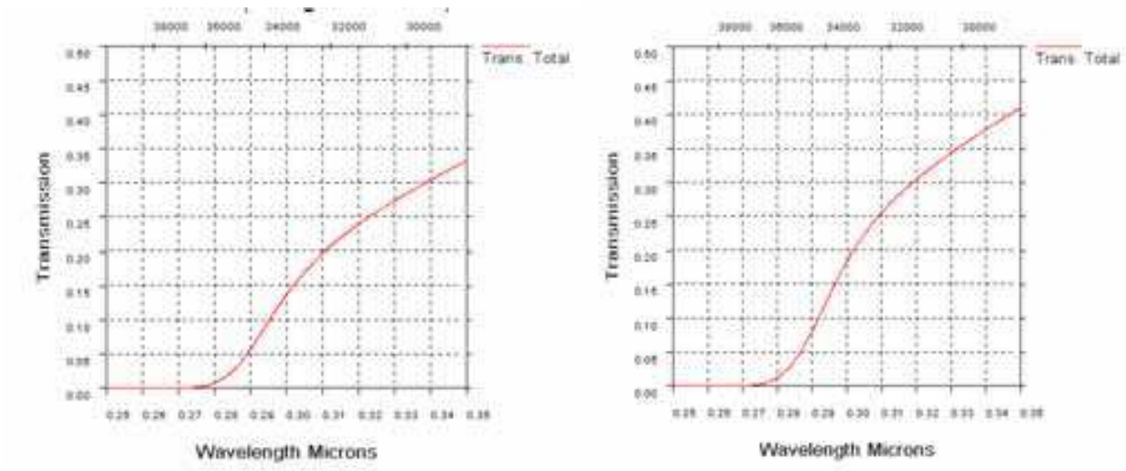

(a) (b)

Fig. 22. UV atmospheric transmission over a slanted path at 15° elevation in clear maritime conditions, 10 km range (22a). UV transmission over a slanted path at 30° elevation in clear maritime conditions, 10 km range (22b)

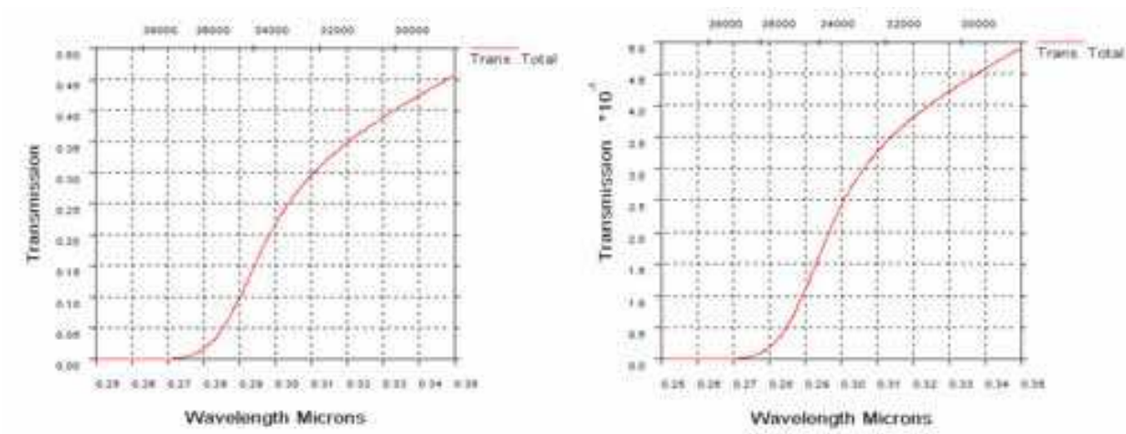

(a) (b)

Fig. 23. UV transmission over a slanted path at 45° elevation in clear maritime conditions, 10 km range (23a). UV atmospheric transmission over a slanted path at 60° elevation in clear maritime conditions, 10 km range (23b)

12. Summary

In this chapter, we have discussed growth, fabrication and characterization of ZnO nanostructures materials and devices on a variety of substrates. ZnO nanostructures offer potential for a variety of optical, electronic and biological devices for nanoscale applications. The Zinc oxide nanostructures are also attractive for energy generation devices and photovoltaic applications. Significant research effort is underway on ZnO nanostructures, their unique properties for application in transparent electronics, ultraviolet (UV) light emitters, piezoelectric devices, chemical sensors and spin electronics.

An assortment of ZnO nanostructures, such as nanorods, nanotubes and nanorings, have been successfully grown via a variety of methods including chemical vapor deposition, thermal evaporation, hydrothermal technique, sol-gel and electro-deposition. These nanostructures have been evaluated for electronic devices, UV detectors, light emitting diodes, lasers, gas sensors, and other biological applications. Further work is underway that will enhance our understanding of ZnO nanostructures and their applications for future system applications.

13. Acknowledgement

The authors would like to acknowledge the contributions of many students at Georgia Tech that have over the years contributed to the exciting work, which has been published by them and presented here in the chapter. We would also like to acknowledge the modeling effort by Dr. John Zeller of NUWC, Newport, RI. The authors would also like to acknowledge the financial support by numerous agencies that have contributed to the ZnO nanostructures and their applications.

14. References

[1] J. R. Choi and Dennis. L. *Polla Journal of Micromechanical Micro-engineering* Volume 3, 60-64, 1993
[2] E. J. Egerton, A. K. Sood, R. Singh, Y. R. Puri, R. F. Davis, J. Pierce, D. C. Look and T. Steiner, *Journal of Electronic Materials* Vol.34, No.6, 2005
[3] Z. L. Wang , A Review Paper, *Journal of Physics: Condensed Matter* 16, 829-858, 2004
[4] X. Wang, J. Song, C. J. Summers, J. H. Ryou, P. Li, R. D. Dupuis, and Z. L. Wang , *J Phys. Chem. B*, 110 (2006) 7720-7724
[5] X. Wang , J. Song , P. Li , J. H. Ryou , R. D. Dupuis , C. J. Summers and Z. L. Wang , *J Am. Chem. Soc.*, 127 (2005) 7920-7923
[6] X. Wang, C. J. Summers and Z. L. Wang, *Nano Letters*, 3 (2004) 423-426.
[7] Z. L. Wang and J. Song, *Science*, 312 (2006) 242-246
[8] Z. Fan and J.G. Lu, *Journal of Nanoscience and Nanotechnology*, Volume 5, 1561-1573 (2003)
[9] R.S. Yang, Y. Ding and Z.L. Wang, *Nano Lett.*, 4, 1309 (2004)
[10] A.K. Sood, Y.R. Puri, P. Gao, C. Lao, Z.L. Wang, D.L. Polla, M.B. Soprano, *Proceedings of SPIE*, Volume 6556, 6556IL (2007)
[11] L. Luo, B. Sosnowchik and L.W. Lin, *Applied Physics Letters* 90, 093101 (2007)
[12] W. Lee, M. C. Jeong and J.M. Myoung, *Acta Materialia*, 52, 3949-3957(2004)
[13] J. B. Baxter and E.S. Aydil, *Journal of Electrochemical Society*, 156 (1), H52-H58 (2009)
[14] P. X. Gao and Z. L. Wang, *J Phys. Chem.* B 106, 12653 (2002)
[15] P. X. Gao, Y. Ding and Z. L. Wang, *Nano Lett.* 3, 1315 (2003)
[16] Z. W. Pan, Z. R. Dai and Z. L. Wang, *Science* 291, 1947(2001)
[17] M. H. Huang, Y. Y. Wu, H. Feick, N. Tran, E. Weber and P. D. Yang, *Adv. Mater.* 13, 113 (2001)
[18] M. S. Arnold, P.H. Avouris, Z. W. Pan and Z. L. Wang, *J Phys. Chem.* B 107, 659 (2003)
[19] Y. Cui and C. M. Lieber, *Science* 291, 851 (2001)
[20] P. G. Collins, M. S. Arnold and Ph. Avouris, *Science* 292, 706 (2001)
[21] J. Kong, N. Franklin, C. Wu, S. Pan, K. J. Cho and H. Dai, *Science* 287, 622 (2000)
[22] Wang, X.D., Ding, Y. Summers, C.J. and Wang, Z.L., *J Phys. Chem. B*. 108, 8773 (2004)

[23] X. Bai, E. G. Wang, P. Gao and Z. L. Wang, *NanoLetters*, 3, 1147 (2003)
[24] P. M. Morales and C. M. Lieber, *Science* 279, 208 (1998)
[25] G.F. Zheng, F. Patolsky, Y. Cui, W.U. Wang, and C.M. Lieber, *Nature Biotechnology* 23 (2005) p. 1294
[26] X.D. Bai, P.X. Gao, Z.L. Wang and E.G. Wang, *Appl. Phys. Letts.* 82, p. 4806 (2003)
[27] Z. L. Wang, and J. H. Song, *Science* 312 , p. 242 (2006)
[28] J.H. Song, J. Zhou, and Z.L. Wang, *Nano Lett.* 6 p. 1656 (2006)
[29] M.H. Zhao, Z.L. Wang, and S.X. Mao, *Nano Lett.* 4 (2004) p. 587
[30] Z.L. Wang, X.Y. Kong, and J.M. Zuo, *Phys. Rev. Letts.* 91 (2003) p. 185502
[31] Z.L. Wang and J. H. Song, *Science*, 312 , 242-246 (2006)
[32] P.X. Gao, J.H. Song, J. Liu and Z.L. Wang, *Advanced Materials*, 19, 67-72 (2006)
[33] X.D. Wang, J.H. Song, J. Liu and Z.L. Wang, *Science*, 316, 102-105 (2007)
[34] D. Sridhar, J. Xie, J.K. Abraham, V. K. Varodan and S.H. Choi, *Proceedings of SPIE*, Volume 6172 (2006)
[35] W. J. F. Beck, L. H. Slooft, M. J. Wienk, J. M. Kroon, and R.A. J. Janssen, *Proceedings of SPIE*, Volume 5938 (2005)
[36] A. M. Piero, P. Ravirajan, K. Govender, D.S. Boyle, P.O. O'Brien, D.C. Bradley, J. Nelson and J.R. Durrant, *Proceedings of SPIE* , Volume 5938 (2005)
[37] J. R. Baxter and E.S. Aydil, *Applied Physics Letters*, 86, 053114 (2005)
[38] For Silicon Solar Cells, i.e. Evergreen Solar (Marlboro, MA), Schott Solar (Burlington, MA), and other Silicon Solar Cell Manufacturers). The cell efficiency varies from 14-18 percent for Polysilicon to Single Crystal Silicon Solar Cells.
[39] T. Takamoto, E. Ikeda, H. Kurita and M. Ohmori, *Applied Physics Letters*, 70, 381 (1997)
[40] J. Wu, W. Walukiewicz, K. M. Yu, W. Shan, J. W. Ager, E.E. Haller, H. Lu, W.J. Schaff, W.K. Metzer and S. Kurtz, *Journal of Applied Physics*, Volume 94, 6477 (2003)
[41] G. Ganguly, D.E. Carlson, S. S. Hyedus, D. Ryan , R. Gordon, D. Pang and R. C. Reedy, *Applied Physics Letters* 85, p 479 (2004)
[42] Z. Longyue, D. Songyuan, X. Weiwei and K. Wang, *Plasma Science and Technology*, Volume 8, No2, March 2006
[43] J. Zeller and T. Manzur, *Proceedings of SPIE*, Volume 7833, 783313 (2010)

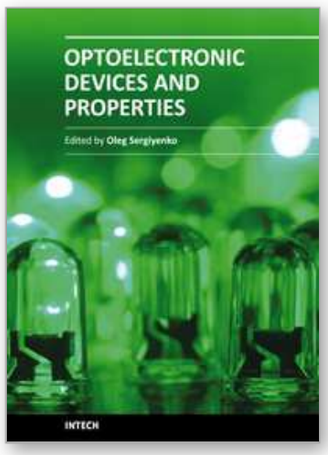

Optoelectronic Devices and Properties

Edited by Prof. Oleg Sergiyenko

ISBN 978-953-307-204-3
Hard cover, 660 pages
Publisher InTech
Published online 19, April, 2011
Published in print edition April, 2011

Optoelectronic devices impact many areas of society, from simple household appliances and multimedia systems to communications, computing, spatial scanning, optical monitoring, 3D measurements and medical instruments. This is the most complete book about optoelectromechanic systems and semiconductor optoelectronic devices; it provides an accessible, well-organized overview of optoelectronic devices and properties that emphasizes basic principles.

How to reference

In order to correctly reference this scholarly work, feel free to copy and paste the following:

Ashok K. Sood, Zhong Lin Wang, Dennis L. Polla, Nibir K. Dhar, Tariq Manzur and A.F.M. Anwar (2011). ZnO Nanostructures for Optoelectronic Applications, Optoelectronic Devices and Properties, Prof. Oleg Sergiyenko (Ed.), ISBN: 978-953-307-204-3, InTech, Available from: http://www.intechopen.com/books/optoelectronic-devices-and-properties/zno-nanostructures-for-optoelectronic-applications

INTECH
open science | open minds

InTech Europe
University Campus STeP Ri
Slavka Krautzeka 83/A
51000 Rijeka, Croatia
Phone: +385 (51) 770 447
Fax: +385 (51) 686 166
www.intechopen.com

InTech China
Unit 405, Office Block, Hotel Equatorial Shanghai
No.65, Yan An Road (West), Shanghai, 200040, China
中国上海市延安西路65号上海国际贵都大饭店办公楼405单元
Phone: +86-21-62489820
Fax: +86-21-62489821

IntechOpen